Published in final edited form as:
J Mol Cell Cardiol. 2012 May ; 52(5): 1074–1082. doi:10.1016/j.yjmcc.2012.01.005.

Partial Restoration of Cardio-Vascular Defects in Rescued Severe Model of Spinal Muscular Atrophy

Monir Shababi[1,7,*], **Javad Habibi**[2,6,*], **Lixin Ma**[3,6], **Jacqueline Glascock**[4,7], **James R. Sowers**[2,5,6], and **Christian L. Lorson**[1,4,7]

[1]Department of Veterinary Pathobiology, University of Missouri, Columbia, MO, 65211

[2]Department of Internal Medicine, University of Missouri, Columbia, MO, 65211

[3]Department of Radiology, University of Missouri, Columbia, MO, 65211

[4]Department of Molecular Microbiology and Immunology, University of Missouri, Columbia, MO, 65211

[5]Department of Medical Pharmacology and Physiology, University of Missouri, Columbia, MO, 65211

[6]Harry S. Truman Veterans Affairs Medical Center, University of Missouri, Columbia, MO, 65211

[7]Bond Life Sciences Center, University of Missouri, Columbia, MO, 65211

Abstract

Spinal muscular atrophy (SMA) is a leading genetic cause of infantile death. Loss of a gene called Survival Motor Neuron 1 (SMN1) and, as a result, reduced levels of the Survival Motor Neuron (SMN) protein leads to SMA development. SMA is characterized by the loss of functional motor neurons in the spinal cord. However, accumulating evidence suggest the contribution of other organs to the composite SMA phenotype and disease progression. A growing number of congenital heart defects have been identified in severe SMA patients. Consistent with the clinical cases, we have recently identified developmental and functional heart defects in two SMA mouse models, occurring at embryonic stage in a severe SMA model and shortly after birth in a less severe model (SMNΔ7). Our goal was to examine the late stage cardiac abnormalities in untreated SMNΔ7 mice and to determine whether gene replacement therapy restores cardiac structure/function in rescued SMNΔ7 model. To reveal the extent of the cardiac structural/functional repair in the rescued mice, we analyzed the heart of untreated and treated SMNΔ7 model using self-complementary Adeno-associated virus (serotype 9) expressing the full-length SMN cDNA. We examined the characteristics of the heart failure such as remodeling, fibrosis, oxidative stress, and vascular integrity in both groups. Our results clearly indicate that fibrosis, oxidative stress activation, vascular remodeling, and a significant decrease in the number of capillaries exist in the SMA heart. The cardiac structural defects were improved drastically in the rescued animals,

Corresponding Author: Christian L. Lorson, Ph.D.,Department of Veterinary Pathobiology, Life Sciences Center, Room 471G, University of Missouri, Columbia, MO 65211 USA, Phone: 573 884-2219, Fax: 573 884-9395, lorsonc@missouri.edu. Co-corresponding Author: Monir Shababi, Ph.D., shababim@missouri.edu.
*These authors contributed equally to this work.

Conflict of interest statement
None declared.

however, the level of impairment was still significant compared to the age-matched wildtype littermates. Furthermore, functional analysis by in vivo cardiac magnetic resonance imaging (MRI) revealed that the heart of the treated SMA mice still exhibit functional defects. In conclusion, cardiac abnormalities are only partially rescued in post-birth treated SMA animals and these abnormalities may contribute to the premature death of vector-treated SMA animals with seemingly rescued motor function but an average life span of less than 70 days as reported in several studies.

Keywords

SMA; scAAV9; Cardiac function; Oxidative stress; Vascular remodeling; MRI

1. Introduction

Spinal muscular atrophy (SMA) is the leading genetic cause of infantile death and is characterized by the loss of the α-motor neurons in the spinal cord [1]. The clinical spectrum is broadly categorized based upon disease onset and physical milestones [2]. SMA results from the loss of *survival motor neuron-1* (*SMN1*) [3]. A human-specific copy gene is present on the same chromosome called *SMN2* [3,4]. *SMN2* is nearly identical to *SMN1* and generates low levels of full-length SMN. *SMN2* cannot prevent disease development in the absence of *SMN1* since the majority of *SMN2*-derived transcripts are alternatively spliced and encode an unstable protein [5,6].

The fundamental pathology in SMA is neurodegeneration, however, there are clinical reports demonstrating the contribution of other tissues to the overall phenotype in the most severe forms (Type 0 and Type I). In severe SMA, several congenital heart defects have been documented including atrial septal defects, dilated right ventricle, ventricular septal defects, and hypoplastic left heart syndrome [7–9]. Sudden death without a clear explanation can occur in severe SMA patients [10]. Central apnea due to bulbar dysfunction and respiratory complications is suggested to be the possible cause of sudden death, even though it also occurs in patients with ventilation support [10]. Therefore, vagal hypertonia induced bradycardia has also been considered [10]. Furthermore, palpitations, ST-segment abnormalities, couplets, diastolic dysfunction, and right ventricular overload have been reported in SMA patients [11,12]. Distal necrosis has also been documented in severe SMA, occasionally with atrial septal defects and asymmetric left ventricular hypertrophy [13,14]. Similar pathologies have been observed in SMA mice treated with therapeutic compounds or viral vectors [15,16]. Life span extension of treated SMA mice has led to increased recognition of distal necrosis in the tail or ear pinna. These results suggest that the dysfunction of the autonomic nervous system may lead to impaired regulation of vascular tone and possibly fetal vasculature defects which cannot be completely restored with post-birth treatments. Recently, our lab and others have identified functional and structural heart defects in SMA animal models [17–19]. Bradycardia is the most common autonomic nervous system phenotype reported in these studies. We have identified cardiac defects occurring during embryonic development in a severe SMA mouse model and shortly after birth in a slightly less severe model (SMNΔ7), suggesting that cardiac defects precede motor neuron degeneration.

Recently, intravenous delivery at postnatal day 1 (P1) of scAAV9 expressing full-length SMN cDNA in SMNΔ7 mice led to a profound phenotypic rescue by restoring motor function/neuromuscular physiology and extended survival up to 250 days [20]. The same group reported complete restoration of the heart rate and partial repair of cardiac function in AAV9-injected animals at P14 [17]. Additional groups reported a significantly extended life

span using a similar vector, however, sudden deaths, respiratory complications, and average life spans of only 65–70 days were common [21,22]. To provide a more detailed analysis of the cardiac defects in these important disease models, we have examined remodeling, fibrosis, oxidative stress, and vascular impairments. In each instance, the SMA mice were profoundly impaired compared to healthy animals and these results served as an important baseline from which we could quantitatively assess cardiac structure/function following SMN gene replacement. To directly compare the functional parameters, we carried out in vivo MRI on the heart of the rescued and age-matched wildtype littermates. Our study demonstrates that the heart of the rescued SMA mice, albeit drastically improved compared to untreated mice, still exhibits structural and functional defects compared to age-matched wildtype mice, suggesting that cardiac defects contribute to the shortened life span of scAAV-rescued mice [21,22].

2. Materials and methods

2.1. SMA animals and injection

All animal experiments took place in accordance with procedures approved by NIH guidelines and MU Animal Care and Use Committee (ACUC). SMNΔ7 animals (*mSmn−/−*, *hSMN2+/+*, *SMNΔ7+/+*) were genotyped at P1[23]. scAAV9 expressing the full-length SMN cDNA was purified by CsCl centrifugation [20] and SMNΔ7 P2 mice were injected intravenously into the temporal facial vein with 1×10^{11} viral genomes.

2.2. Histology

Animals were anesthetized using 0.06ml/g isoflurane (Vet One) for 3–5 minutes (adequacy of anesthesia was verified by lack of a twitch after pulling the hind limb), euthanized, hearts were harvested, and immersed in 60mM KCl to arrest the heart in diastolic stage before fixation in 4% paraformaldehyde. 4μm VVG-stained cross-sections were prepared at the MU Veterinary Medical Diagnostic Laboratory. Cardiac remodeling and interstitial fibrosis was quantified using MetaVue as previously described [19] and provided as supplement.

2.3. Western blot

Heart and spinal cord tissues were immediately placed in liquid nitrogen post-harvest, and kept in −80°C until protein extraction. 100 mg of tissue was homogenized in 200–500μl of JLB buffer; equal amounts of protein were loaded onto 10–15% SDS-PAGE gel as described [24]. Blots were incubated overnight at 4°C with: mouse anti-SMN (BD-Bioscienc es), rabbit anti-AngII (Novus-Biologicals), mouse anti-P47-phox, rabbit anti-AT1R and anti-Nox2 (Santa Cruz-Biotechnology). TrueBlot™ Ultra HRP anti-mouse IgG (eBioscience) and HRP anti-rabbit IgG (Jackson-Immunoresearch) were secondary antibodies. Blots were visualized by chemiluminescence, images were captured by Fugi-Imager, LAS-3000, and quantified by Multi-Gauge/V2.3. Blots were stripped with 30% H_2O_2/PBS (1:1) and reprobed with rabbit anti-β-actin or anti-IP90, and mouse anti-tubulin.

2.4. 3-Nitrotyrosine immuno-staining

3-Nitrotyrosine was quantified as previously described [25]. Sections were incubated with rabbit anti-nitrotyrosine (Chemicon) overnight, washed and incubated with secondary antibodies, biotinylated linked, and labeled with streptavidin for 30 minutes. After several TBST rinses, diaminobenzidine was applied (5 minutes), rinsed, stained with hematoxylin (45 seconds), washed, rehydrated in ethanol series and citrisolve, and mounted with Permount (Fischer).

2.5. Immunohistochemistry

Double immunostaining of the vasculature has been previously described [26]. Paraffin sections were immuno-labeled for smooth muscle cells and endothelial cells using α-smooth muscle actin (MO851, Dako) and α-eNOS (BD-Biosciences), respectively. Endothelial cells of arterioles and capillaries were stained with mouse anti-von Willibrand factor (vWF) (Santa Cruz-Biotechnology). Cardiomyocytes were stained with 10μg/ml of FITC-tagged Wheat Germ Agglutinin (Invitrogen) and immunostained with goat PCNA and rabbit Caspase 3 (Santa Cruz-Biotechnology). Images were captured using a bi-photon confocal microscope (Zeiss LSM, 510/MLO) under the same computer settings for all sections in each experiment. The width of media in arterioles, capillary numbers per total area, gray scale intensities, and cross-sectional area of myocytes were measured by MetaVue and MetaMorph.

2.6. In vivo MRI

Noninvasive MRI scans were performed using a 7 Tesla/210 mm horizontal-bore MRI (Agilent/Varian) as previously described [27]. 5–6 consecutive short-axis slices, imaged from basal to apical for covering the entire LV were acquired at 16 equally-spaced time points throughout the entire cardiac cycle with a frame rate of 8–12 ms/frame. Segment software was used for quantitative measurements of LV functional parameters [28]. A detailed procedure is provided as a Supplement.

2.7. Statistics

All results are presented as means + standard error and *P* value was determined by unpaired two-tailed *t* test. Bonferroni correction was applied to emphasize the significant differences between the groups in multiple comparisons by reducing the threshold significance from <0.05 to <0.01.

3. Results

3.1. Gene replacement therapy rescues cardiac remodeling

A widely utilized SMA mouse model is referred to “SMNΔ7”. SMNΔ7 model lacks murine *Smn*, contains two copies of human *SMN2*, and includes an additional transgene expressing SMNΔ7 cDNA (*mSmn*$^{-/-}$, *h SMN2* $^{+/+}$, SMNΔ7$^{+/+}$) with a life span of 14–16 days [29]. To obtain rescued SMA mice, 1×10^{11} genomic copies of scAAV9-SMN, a vector expressing the full-length SMN cDNA, was intravenously (IV) injected into SMNΔ7 mice. This delivery mode allows distribution of the virus to the central nervous system as well as periphery organs, including heart [20,30]. The scAAV9-treated mice demonstrate a significant increase in their life span and weight gain compared to untreated mice (Fig.1A, B, $P<0.0001$).

Previously, we observed the initiation of interventricular septum (IVS) remodeling in SMNΔ7 animals at P3-5, resulting in highly dilated ventricles by P9 [19]. Using bright field images of Verhoeff-van Gieson (VVG) stained heart sections, we compared the IVS width in untreated SMNΔ7 hearts at P14, scAAV9-SMN treated hearts at P23, and wildtype hearts at both time points. Untreated SMA animals do not survive until P23 and could not be included at this time point. Our results revealed that IVS remodeling in SMA hearts at P14 is even further exacerbated at this later stage (Fig.1C). Interestingly, the IVS of the rescued animals at P23 closely resembled that of the wildtype heart at P14 but was still significantly thinner than the IVS of the age-matched wildtype at P23, suggesting that IVS remodeling is still initiated in the treated animals, but the degree of remodeling is reduced (Fig.1C). To determine whether apoptosis or alterations in cell division are responsible for IVS remodeling, we quantified the level of Caspase 3 and PCNA in the IVS region and found no

difference in the level of these proteins between groups (Supplemental Fig. 1A, B). Therefore, we measured the cross-sectional area of the WGA-labeled cardiomyocytes at P14 and demonstrated a significant reduction in the size of SMA cardiomyocytes which most likely contributes to IVS remodeling. Cardiomyocytes sizes are restored in the rescued mice to the levels of P14 wildtype but still significantly smaller than age-matched wildtype, which directly correlates to IVS thickness (Fig. 1D).

3.2. Increased Oxidative Stress and 3-nitrotyrosin may contribute to interstitial fibrosis in the SMA heart

Development of cardiac fibrosis is derived from an imbalance in the synthesis and degradation of the extracellular matrix, which is composed predominantly of collagens type I and III. A shift in the collagen type I/III ratio results in a buildup of collagen type III which has been implicated in myocardial stiffness and the progression of heart failure [31]. VVG stains collagen type III pink; therefore, the intensity of the pink area indicates the degree of interstitial fibrosis (Fig. 2A). In SMNΔ7 mice, fibrosis initiates at P2 and progresses rapidly to P9 [19]. Direct comparison between the untreated, treated, and age-matched wildtype mice, demonstrates that the level of fibrosis in the SMA heart is significantly intensified by P14 (Fig. 2A). As expected, scAAV9-SMN treated hearts exhibit very low levels of fibrosis at P23. The level of fibrosis in the rescued animals at P23 is similar to that observed in wildtype animals at P14 and P23 (Fig. 2A). These results demonstrate that interstitial fibrosis is attenuated by scAAV9-SMN treatment.

One of the underlying mechanisms for cardiac fibrosis is oxidative stress [32,33], which is caused by high levels of reactive oxygen species (ROS) and contributes significantly to the pathogenesis of heart failure [34]. ROS are generated from many sources including uncoupled nitric oxide synthases (eNOS), and NADPH oxidase [35,36]. Oxidation of proteins is marked by an increase in 3-nitrotyrosin (3-NT) content which takes place by binding of peroxynitrate (ONOO-) to tyrosine residues of proteins [37]. To determine whether increased 3-NT levels contribute to fibrosis, we quantified the cardiac 3-NT content by immunohistochemistry and determined that it was significantly higher in P9 SMA hearts compared to wildtype (Fig. 2B). Consistent with the other phenotypic parameters of the rescued SMA heart, the 3-NT level was reduced in the rescued animals at P23 compared to untreated and was similar to that of the baseline levels detected in wildtype at P9 and P23 (Fig. 2B).

3.3. Oxidative stress mediated by NADPH-oxidase is abolished in the rescued hearts

To further examine the potential source of ROS that may contribute to cardiac fibrosis in SMNΔ7 mice, we quantified the levels of Ang-II and the major subunits of NADPH-oxidase in the heart. Ang-II is one of the most important biomarkers that stimulates the NADPH oxidase enzyme and plays a key role in vasoconstriction, fibrosis, and remodeling [38–40]. Most adverse biological effects of Ang-II are mediated by the AT1 receptor (AT1R) subtype [41]. Involvement of NADPH oxidase can be determined by quantifying the expression levels of three major subunits of the NADPH oxidase complex: Nox2, Rac1, and p47-phox. We have previously demonstrated a significant increase in the levels of Ang-II, AT1R, Rac1, and Nox2 immuno-staining in SMA hearts by P9 [19]. In this report, we use Western blot to verify that a severe reduction of SMN in the heart (Fig. 3A) leads to a significant increase in the levels of the NADPH-oxidase subunits at P9 or 14 (Fig. 3B, C, D, E, F). Conversely, delivery of scAAV9-SMN significantly increases the SMN levels in the heart (Fig. 4A), and thereby reestablishes the oxidative stress biomarkers to wildtype levels (Fig. 4B, C, D, E, F). The apparent low SMN levels in the wildtype heart at P23 is due in part to the short exposure required to capture the exceedingly high SMN levels in the scAAV9-

SMN treated hearts, and that SMN expression decreases significantly beyond neonatal stages [42].

The involvement of NADPH oxidase in motor neuron degeneration has been reported in ALS mice [43]. To investigate whether NADPH oxidase activation occurs in the spinal cord at symptomatic stages, we quantified the expression levels of Ang-II, AT1R, and NADPH-oxidase subunits in the spinal cord at P12. Interestingly, there were no differences between the SMA mice and the age-matched wildtype regarding the level of these proteins in the spinal cord (Supplemental Fig. 2). These results demonstrate that the NADPH oxidase-mediated oxidative stress occurs in SMA heart but, in contrast to ALS mice, does not appear to play a role in SMA motor neuron degeneration.

3.4. Vascular remodeling and loss of capillaries occur in SMA heart and is improved in the rescued hearts

Potential vascular system abnormalities exist in SMA as suggested by distal necrosis in severe SMA patients and mice models [13–16] and arterial wall remodeling in SMNΔ7 mice [19]. Therefore, we examined vascular integrity. To identify the specific layer of the arterial wall that has been remodeled, we double-stained P9 heart sections with anti-eNOS to distinguish the endothelial cells in intima and anti-smooth muscle actin to specify the smooth muscle cells (SMCs) in media. Confocal images of SMA heart sections revealed a loss of SMCs, leading to a reduction in the medial thickness of arterioles (Fig. 5A). As expected, the SMCs were restored in arterioles of the rescued animals at P23, resulting in medial thickness almost equivalent to P9 wildtype mice and similar to the age-matched wildtype hearts at P23 (Fig. 5A). Additionally, the intensity of eNOS was measured in the intima of arterioles, however, eNOS levels were similar in untreated SMA and wildtype (Supplemental Fig. 3A), indicating that the integrity of the endothelial cells was not damaged at P9.

Transfer of oxygenated blood from the arterioles to tissue cells is directed by functional capillary bed. Within the mouse heart, von Willebrand factor (vWF) is expressed specifically in a subpopulation of cardiac microvascular endothelial cells [44]. Therefore, we used fluorescence immunohistochemistry to quantify the density of vWF-positive capillaries in the heart. Our confocal images of SMA heart sections at P9 demonstrate a significantly reduced number of vWF-expressing capillaries compared to wildtype heart (Fig. 5B). Interestingly, the average number of capillaries was higher in the rescued hearts compared to untreated and similar to the levels of the wildtype at P9. However, the number of capillaries in the rescued hearts was still less than that in the wildtype heart at P23 (Fig. 5B). To determine that the loss of capillaries is not due to the loss of vWF in general, we quantified the vWF levels in the endothelial cells of arterioles and found no difference in the vWF intensity (Supplemental Fig. 3B), suggesting that cardiac capillaries are indeed reduced in number.

3.5. Cine MRI measurements of cardiac function in rescued SMA mice demonstrate defects

To perform measurements of cardiac function, cine MRI was conducted within the fourth week of life for rescued and age-matched wildtype mice. Untreated SMA mice were no longer alive at the selected time point. Short axis cine images (Fig. 6A) were captured to quantify left ventricle (LV) volumes using Segment [28] to determine: 1) stroke volume (the volume of blood pumped with each contraction); 2) LV ejection fraction (the fraction of blood pumped out of the left ventricle with each heart beat); 3) cardiac output (the volume of blood pumped by the heart per minute); 4) LV myocardial mass [45], and 5) septal wall thickness [46]. The heart rate was assessed through ECG monitoring during cardiac MRI. The rescued SMA mice demonstrated insufficient cardiac function indicated by a decreased

heart rate, stroke volume, cardiac output, and ejection fraction compared to the age-matched wildtype (Fig. 6B, C, D, E). LV myocardial mass and interventricular septal wall thickness were also significantly lower in the rescued SMA mice than wildtype (Fig. 6F, G) which is consistent with the microscopy results (Fig. 1C). Collectively, these data demonstrate that the heart in treated SMA mice still performs inadequately as interpreted by cine MRI evaluation, even though there are significant improvements at the cellular and biochemical levels in the rescued hearts.

4. Discussion

Gene replacement with scAAV-SMN has provided the most substantial correction in severe SMA mice [15,20–22]. However, there were intriguing distinctions regarding the survival rate between the various studies. Interestingly, SMN delivered by scAAV8 via intracerebroventricular injection led to a partial phenotypic rescue with a shorter average life span than systemic injection of scAAV9-SMN [15,20]. This difference may be due to: 1) the ability of scAAV9 to provide global cardiac gene transfer superior to AAV8 [47,48], or 2) increased cardiac transduction efficiency inherent to IV versus ICV administration, or both. However, even sufficient levels of cardiac transduction post-birth may not result in complete rescue if SMN is required for embryonic heart and/or autonomic development. Two studies reported similar results in which IV administration of scAAV9-SMN significantly restored motor function but only extended average life span to approximately 65–69 days, suggesting that other organ systems were not functioning properly [21,22].

We have previously demonstrated that cardiac structural defects precede motor neuron defects in two severe models of SMA. Here we detail the late-stages of cardiac pathology in SMNΔ7 mice, including fibrosis, oxidative stress, remodeling, and identify a novel pathophysiological component: vascular abnormalities, including medial thinning in coronary arterioles and loss of capillaries. Arterioles branch into capillary beds and supply the heart muscles with oxygenated blood. The contractility of SMCs in the media of arterioles changes the volume of blood vessels and the local blood pressure generated against vessel walls. Therefore, the thin layer of SMCs and decreased density of capillary beds in the SMA hearts seriously impacts the blood supply to cardiomyocytes and consequently, to the entire body. Importantly, reduced growth of cardiomyocytes in SMA heart can be caused by diminished capillaries leading to IVS remodeling, even though we cannot rule out alternative apoptotic pathways.

To determine the extent that the cardiac abnormalities can be corrected in the rescued animals, we compared each component of the cardiac pathology in untreated, vector-treated, and age matched wildtype mice. The results demonstrate that much of the cardiopathology in the rescued mice at P23 has been significantly improved, albeit to levels comparable to those present in P9–P14 wildtype mice. This is consistent with the body weight of the rescued SMA mice whose weight at P23 is comparable to wildtype mice at P9 (Fig.1B). These results imply that gene replacement therapy at P2 leads to a gradual correction of pathological symptoms in the heart, and possibly other tissues/organs, which is still developmentally delayed compared to the age-matched wildtype mice. Interestingly, 3–4 fold higher SMN levels in the heart of the rescued mice, compared to wildtype, has not led to restoration of all the abnormalities except for 1) the level of oxidative stress biomarkers which correlates to very low levels of fibrosis, and 2) medial thickness. These results suggest a crucial role for SMN during embryonic development in this severe model and are consistent with elevated SMN levels during embryonic development compared to post-natal days [42,49].

Oxidative stress plays a major role in congestive heart failure in human and cardiac dysfunction of the *mdx* mouse model of Duchenne Muscular Dystrophy [50,51]. We have indicated that the level of the NADPH oxidase subunits in the spinal cord of SMA mice at P12 was unaltered (as opposed to the SMA heart) which is in contrast with observations in ALS mice [43]. Similarly, 3-NT deposition could not pathologically be detected in motor neurons of SMA type 1 autopsy samples [52]. Our data suggest that increased 3-NT content and NADPH-oxidase activation is heart-specific and is not a general phenomenon of neurodegenerative diseases occurring in every tissue at end-stage. In addition, not all of the oxidative stress pathways are activated in SMA, as we did not detect any increase in the level of superoxide dismutase (SOD) in SMA hearts.

Similar to the partial restoration of cardiac structure in rescued animals, the level of heart function measured by cine MRI, is still lower than the ideal level compared to the wildtype animals. However, some of the structural abnormalities in the rescued mice are relatively modest and are unlikely to fully explain the more profound functional abnormalities. The functional abnormalities are consistent with the previously reported results in which highly sensitive echocardiography was utilized to measure cardiac function in SMA mice at P14 [17]. The only functional parameter that was completely restored in their P14 rescued animals was bradycardia, which still exists in our rescued mice. However, the level of cardiac output and stroke volume in their animals at P14 is comparable to our rescued mice at fourth week of age. The discrepancies could be attributed to differences in viral titer, age of animals, and the type of functional analysis. Bevan et al. demonstrated that contractile dysfunction still exists in rescued mice with totally rescued heart rate, and in untreated mice after increasing the heart rate with dobutamine treatment [17]. Therefore, it is unlikely that reduced contractility in our rescued SMA hearts is entirely due to bradycardia. It will be important to further examine these defects to provide a more comprehensive understanding of SMA cardiac pathology, including demonstration of decreased contractility in isolated myocytes and/or heart preparations to conclusively determine the underlying basis of contractile defects. A possible explanation is impaired contractile reserve due to low metabolic ATP reserve. Abnormalities in ATP-generating pathways (mitochondrial function, glycolysis, glycogenolysis, and the phosphotransferase reactions) can reduce ATP supply in failing hearts [53]. Abnormal cardiac mitochondria and hypoglycemia in SMA mice and patients are reported [17,54,55]. Nevertheless, the main conclusion of both types of analysis is that cardiac function cannot be fully rescued with post-birth treatment. In conclusion, our data demonstrates that post-birth restoration of SMN in the heart does not completely rescue the heart defects, suggesting a vital role for SMN during cardiogenesis in utero. It is also likely that autonomic nervous system abnormalities contribute to the observed functional cardiac defects.

Supplementary Material

Refer to Web version on PubMed Central for supplementary material.

Acknowledgments

Funding

This work was supported by grants from the National Institutes of Health, (R01 HL107910-01, R01 HL107910-01 to J.R.S.), a Faculty Research Award from the MU College of Veterinary Medicine to C.L.L. and SMA Europe to M.S.

We would like to thank members of the Lorson lab for their helpful discussions and Dr. Hans Rindt for the generous gift of WGA. In vivo MRI was performed at the Biomolecular Imaging Center supported by the Harry S. Truman Veterans Affairs Hospital at the University of Missouri and we greatly appreciate the technical assistance from Ming Yang.

References

1. Crawford TO, Pardo CA. The neurobiology of childhood spinal muscular atrophy. Neurobiol Dis. 1996; 3:97–110. [PubMed: 9173917]
2. Munsat TL, Davies KE. International sma consortium meeting (26–28 june 1992, bonn, germany). Neuromuscul Disord. 1992; 2:423–428. [PubMed: 1300191]
3. Lefebvre S, Burglen L, Reboullet S, Clermont O, Burlet P, Viollet L, et al. Identification and characterization of a spinal muscular atrophy-determining gene. Cell. 1995; 80:155–165. [PubMed: 7813012]
4. Rochette CF, Gilbert N, Simard LR. Smn gene duplication and the emergence of the smn2 gene occurred in distinct hominids: Smn2 is unique to homo sapiens. Hum Genet. 2001; 108:255–266. [PubMed: 11354640]
5. Lorson CL, Strasswimmer J, Yao JM, Baleja JD, Hahnen E, Wirth B, et al. Smn oligomerization defect correlates with spinal muscular atrophy severity. Nat Genet. 1998; 19:63–66. [PubMed: 9590291]
6. Lorson CL, Hahnen E, Androphy EJ, Wirth B. A single nucleotide in the smn gene regulates splicing and is responsible for spinal muscular atrophy. Proc Natl Acad Sci U S A. 1999; 96:6307–6311. [PubMed: 10339583]
7. Mulleners WM, van Ravenswaay CM, Gabreels FJ, Hamel BC, van Oort A, Sengers RC. Spinal muscular atrophy combined with congenital heart disease: A report of two cases. Neuropediatrics. 1996; 27:333–334. [PubMed: 9050054]
8. Rudnik-Schoneborn S, Heller R, Berg C, Betzler C, Grimm T, Eggermann T, et al. Congenital heart disease is a feature of severe infantile spinal muscular atrophy. J Med Genet. 2008; 45:635–638. [PubMed: 18662980]
9. Moller P, Moe N, Saugstad OD, Skullerud K, Velken M, Berg K, et al. Spinal muscular atrophy type i combined with atrial septal defect in three sibs. Clin Genet. 1990; 38:81–83. [PubMed: 2208769]
10. Ioos C, Leclair-Richard D, Mrad S, Barois A, Estournet-Mathiaud B. Respiratory capacity course in patients with infantile spinal muscular atrophy. Chest. 2004; 126:831–837. [PubMed: 15364763]
11. Finsterer J, Stollberger C. Cardiac involvement in werdnig-hoffmann's spinal muscular atrophy. Cardiology. 1999; 92:178–182. [PubMed: 10754348]
12. Distefano G, Sciacca P, Parisi MG, Parano E, Smilari P, Marletta M, et al. heart involvement in progressive spinal muscular atrophy. A review of the literature and case histories in childhood. Pediatr Med Chir. 1994; 16:125–128. [PubMed: 8078785]
13. Rudnik-Schoneborn S, Vogelgesang S, Armbrust S, Graul-Neumann L, Fusch C, Zerres K. Digital necroses and vascular thrombosis in severe spinal muscular atrophy. Muscle Nerve. 2010; 42:144–147. [PubMed: 20583119]
14. Araujo Ade Q, Araujo M, Swoboda KJ. Vascular perfusion abnormalities in infants with spinal muscular atrophy. J Pediatr. 2009; 155:292–294. [PubMed: 19619755]
15. Passini MA, Bu J, Roskelley EM, Richards AM, Sardi SP, O'Riordan CR, et al. Cns-targeted gene therapy improves survival and motor function in a mouse model of spinal muscular atrophy. J Clin Invest. 2010; 120:1253–1264. [PubMed: 20234094]
16. Avila AM, Burnett BG, Taye AA, Gabanella F, Knight MA, Hartenstein P, et al. Trichostatin a increases smn expression and survival in a mouse model of spinal muscular atrophy. J Clin Invest. 2007; 117:659–671. [PubMed: 17318264]
17. Bevan AK, Hutchinson KR, Foust KD, Braun L, McGovern VL, Schmelzer L, et al. Early heart failure in the smn{delta}7 model of spinal muscular atrophy and correction by postnatal scaav9-smn delivery. Hum Mol Genet. 2010; 19(20):3895–3905. [PubMed: 20639395]
18. Heier CR, Satta R, Lutz C, Didonato CJ. Arrhythmia and cardiac defects are a feature of spinal muscular atrophy model mice. Hum Mol Genet. 2010; 19(20):3906–3918. [PubMed: 20693262]
19. Shababi M, Habibi J, Yang HT, Vale SM, Sewell WA, Lorson CL. Cardiac defects contribute to the pathology of spinal muscular atrophy models. Hum Mol Genet. 2010; 19(20):4059–4071. [PubMed: 20696672]

20. Foust KD, Wang X, McGovern VL, Braun L, Bevan AK, Haidet AM, et al. Rescue of the spinal muscular atrophy phenotype in a mouse model by early postnatal delivery of smn. Nat Biotechnol. 2010; 28(3):271–274. [PubMed: 20190738]

21. Valori CF, Ning K, Wyles M, Mead RJ, Grierson AJ, Shaw PJ, et al. Systemic delivery of scaav9 expressing smn prolongs survival in a model of spinal muscular atrophy. Sci Transl Med. 2010; 2:35ra42.

22. Dominguez E, Marais T, Chatauret N, Benkhelifa-Ziyyat S, Duque S, Ravassard P, et al. Intravenous scaav9 delivery of a codon-optimized smn1 sequence rescues sma mice. Hum Mol Genet. 2011; 20:681–693. [PubMed: 21118896]

23. Coady TH, Baughan TD, Shababi M, Passini MA, Lorson CL. Development of a single vector system that enhances trans-splicing of smn2 transcripts. PLoS One. 2008; 3:e3468. [PubMed: 18941511]

24. Shababi M, Glascock J, Lorson CL. Combination of smn trans-splicing and a neurotrophic factor increases the life span and body mass in a severe model of spinal muscular atrophy. Hum Gene Ther. 2010; 22(2):135–144. [PubMed: 20804424]

25. Habibi J, Hayden MR, Sowers JR, Pulakat L, Tilmon RD, Manrique C, et al. Nebivolol attenuates redox-sensitive glomerular and tubular mediated proteinuria in obese rats. Endocrinology. 152:659–668. [PubMed: 21177830]

26. DeMarco VG, Habibi J, Whaley-Connell AT, Schneider RI, Sowers JR, Andresen BT, et al. Rosuvastatin ameliorates the development of pulmonary arterial hypertension in the transgenic (mren2)27 rat. Am J Physiol Heart Circ Physiol. 2009; 297:H1128–1139. [PubMed: 19633211]

27. Tsika RW, Ma L, Kehat I, Schramm C, Simmer G, Morgan B, et al. Tead-1 overexpression in the mouse heart promotes an age-dependent heart dysfunction. J Biol Chem. 2010; 285:13721–13735. [PubMed: 20194497]

28. Heiberg E, Wigstrom L, Carlsson M, Bolger AF, Karlsson M. Time resolved three-dimensional automated segmentation of the left ventricle. Proceedings of IEEE Computers In Cardiology. 2005; 32:599–602.

29. Le TT, Pham LT, Butchbach ME, Zhang HL, Monani UR, Coovert DD, et al. Smndelta7, the major product of the centromeric survival motor neuron (smn2) gene, extends survival in mice with spinal muscular atrophy and associates with full-length smn. Hum Mol Genet. 2005; 14:845–857. [PubMed: 15703193]

30. Foust KD, Nurre E, Montgomery CL, Hernandez A, Chan CM, Kaspar BK. Intravascular aav9 preferentially targets neonatal neurons and adult astrocytes. Nat Biotechnol. 2009; 27:59–65. [PubMed: 19098898]

31. Lamparter S, Maisch B. significance of matrix metalloproteinases in cardiovascular diseases. Z Kardiol. 2000; 89:949–957. [PubMed: 11098546]

32. Aragno M, Mastrocola R, Alloatti G, Vercellinatto I, Bardini P, Geuna S, et al. Oxidative stress triggers cardiac fibrosis in the heart of diabetic rats. Endocrinology. 2008; 149:380–388. [PubMed: 17901230]

33. Zhao W, Zhao T, Chen Y, Ahokas RA, Sun Y. Oxidative stress mediates cardiac fibrosis by enhancing transforming growth factor-beta1 in hypertensive rats. Mol Cell Biochem. 2008; 317:43–50. [PubMed: 18581202]

34. Soberman RJ. The expanding network of redox signaling: New observations, complexities, and perspectives. J Clin Invest. 2003; 111:571–574. [PubMed: 12618508]

35. Satoh M, Fujimoto S, Haruna Y, Arakawa S, Horike H, Komai N, et al. Nad(p)h oxidase and uncoupled nitric oxide synthase are major sources of glomerular superoxide in rats with experimental diabetic nephropathy. Am J Physiol Renal Physiol. 2005; 288:F1144–1152. [PubMed: 15687247]

36. Saavedra WF, Paolocci N, St John ME, Skaf MW, Stewart GC, Xie JS, et al. Imbalance between xanthine oxidase and nitric oxide synthase signaling pathways underlies mechanoenergetic uncoupling in the failing heart. Circ Res. 2002; 90:297–304. [PubMed: 11861418]

37. Habibi J, DeMarco VG, Ma L, Pulakat L, Rainey WE, Whaley-Connell AT, et al. Mineralocorticoid receptor blockade improves diastolic function independent of blood pressure

reduction in a transgenic model of raas overexpression. Am J Physiol Heart Circ Physiol. 2011; 300:H1484–1491. [PubMed: 21239636]

38. Habibi J, Whaley-Connell A, Qazi MA, Hayden MR, Cooper SA, Tramontano A, et al. Rosuvastatin, a 3-hydroxy-3-methylglutaryl coenzyme a reductase inhibitor, decreases cardiac oxidative stress and remodeling in ren2 transgenic rats. Endocrinology. 2007; 148:2181–2188. [PubMed: 17317778]
39. Sowers JR. Hypertension, angiotensin ii, and oxidative stress. N Engl J Med. 2002; 346:1999–2001. [PubMed: 12075063]
40. Habibi J, Whaley-Connell A, Hayden MR, DeMarco VG, Schneider R, Sowers SD, et al. Renin inhibition attenuates insulin resistance, oxidative stress, and pancreatic remodeling in the transgenic ren2 rat. Endocrinology. 2008; 149:5643–5653. [PubMed: 18653711]
41. Berk, BC. Sci STKE. 2003. Angiotensin type 2 receptor (at2r): A challenging twin; p. PE16
42. La Bella V, Cisterni C, Salaun D, Pettmann B. Survival motor neuron (smn) protein in rat is expressed as different molecular forms and is developmentally regulated. Eur J Neurosci. 1998; 10:2913–2923. [PubMed: 9758161]
43. Wu DC, Re DB, Nagai M, Ischiropoulos H, Przedborski S. The inflammatory nadph oxidase enzyme modulates motor neuron degeneration in amyotrophic lateral sclerosis mice. Proc Natl Acad Sci U S A. 2006; 103:12132–12137. [PubMed: 16877542]
44. Aird WC, Edelberg JM, Weiler-Guettler H, Simmons WW, Smith TW, Rosenberg RD. Vascular bed-specific expression of an endothelial cell gene is programmed by the tissue microenvironment. J Cell Biol. 1997; 138:1117–1124. [PubMed: 9281588]
45. Berr SS, Roy RJ, French BA, Yang Z, Gilson W, Kramer CM, et al. Black blood gradient echo cine magnetic resonance imaging of the mouse heart. Magn Reson Med. 2005; 53:1074–1079. [PubMed: 15844138]
46. Zhang H, Morgan B, Potter BJ, Ma L, Dellsperger KC, Ungvari Z, et al. Resveratrol improves left ventricular diastolic relaxation in type 2 diabetes by inhibiting oxidative/nitrative stress: In vivo demonstration with magnetic resonance imaging. Am J Physiol Heart Circ Physiol. 2010; 299:H985–994. [PubMed: 20675566]
47. Bish LT, Morine K, Sleeper MM, Sanmiguel J, Wu D, Gao G, et al. Adeno-associated virus (aav) serotype 9 provides global cardiac gene transfer superior to aav1, aav6, aav7, and aav8 in the mouse and rat. Hum Gene Ther. 2008; 19:1359–1368. [PubMed: 18795839]
48. Pacak CA, Mah CS, Thattaliyath BD, Conlon TJ, Lewis MA, Cloutier DE, et al. Recombinant adeno-associated virus serotype 9 leads to preferential cardiac transduction in vivo. Circ Res. 2006; 99:e3–9. [PubMed: 16873720]
49. Burlet P, Huber C, Bertrandy S, Ludosky MA, Zwaenepoel I, Clermont O, et al. The distribution of smn protein complex in human fetal tissues and its alteration in spinal muscular atrophy. Hum Mol Genet. 1998; 7:1927–1933. [PubMed: 9811937]
50. Sam F, Kerstetter DL, Pimental DR, Mulukutla S, Tabaee A, Bristow MR, et al. Increased reactive oxygen species production and functional alterations in antioxidant enzymes in human failing myocardium. J Card Fail. 2005; 11:473–480. [PubMed: 16105639]
51. Williams IA, Allen DG. The role of reactive oxygen species in the hearts of dystrophin-deficient mdx mice. Am J Physiol Heart Circ Physiol. 2007; 293:H1969–1977. [PubMed: 17573457]
52. Hayashi M, Araki S, Arai N, Kumada S, Itoh M, Tamagawa K, et al. Oxidative stress and disturbed glutamate transport in spinal muscular atrophy. Brain Dev. 2002; 24:770–775. [PubMed: 12453601]
53. Ingwall JS. Energy metabolism in heart failure and remodelling. Cardiovasc Res. 2009; 81:412–419. [PubMed: 18987051]
54. Bruce AK, Jacobsen E, Dossing H, Kondrup J. Hypoglycaemia in spinal muscular atrophy. Lancet. 1995; 346:609–610. [PubMed: 7651007]
55. Butchbach ME, Rose FF Jr, Rhoades S, Marston J, McCrone JT, Sinnott R, et al. Effect of diet on the survival and phenotype of a mouse model for spinal muscular atrophy. Biochem Biophys Res Commun. 2009; 391:835–840. [PubMed: 19945425]

Highlights

- Rescued SMA mice demonstrate improvements in cardiac structural and cellular pathology.
- Vascular and capillary defects are improved in rescued mice.
- Cine MRI indicates cardiac functional impairments in rescued SMA mice.
- Functional defects are most likely contributing to the premature death of treated SMA mice.

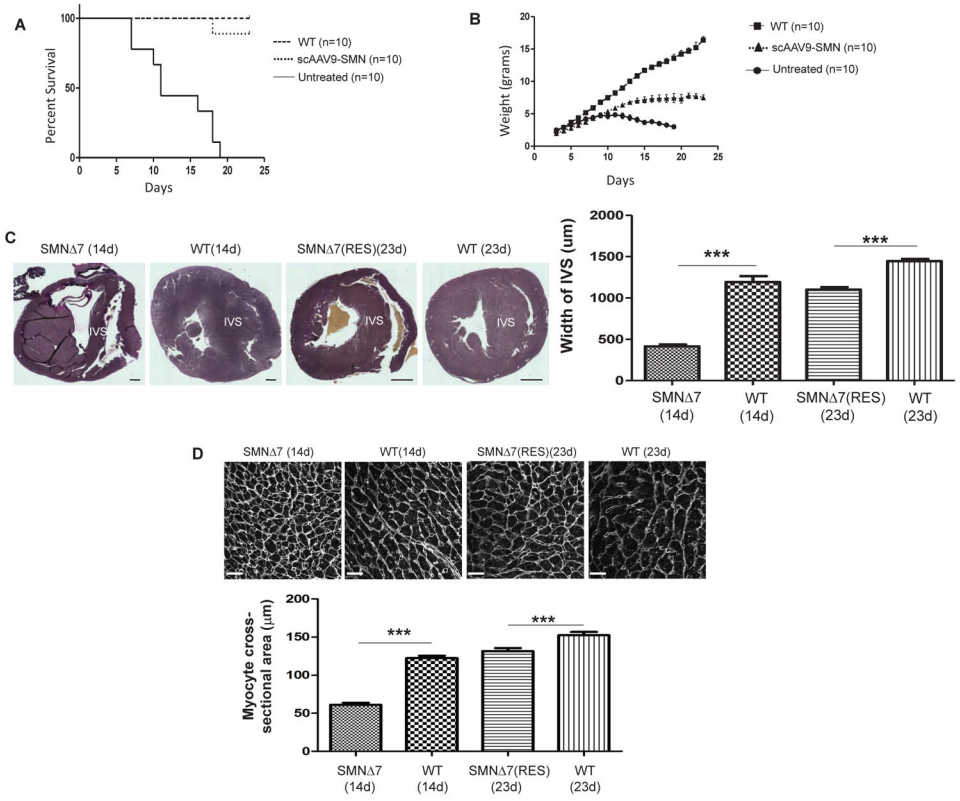

Figure 1.

Gene replacement therapy rescues the SMA phenotype and improves cardiac remodeling. Kaplan-Meier graph indicates percent survival of WT, untreated SMNΔ7, and treated SMNΔ7 using 1×10^{11} genomic copies of scAAV9-SMN at P2 (A). *P* value was determined by log-rank (Mantel-Cox) test ($P<0.0001$). The level of weight gained post-injection until the day of sacrifice was graphed (B). The *p* value was determined by two-tailed t test ($P<0.0001$). Representative VVG-stained heart sections were used to measure the width of interventricular septum, scale bar at P14=200μm; at P23=1mm (C). Representative myocardial sections showing FITC-tagged WGA labeling to quantify the cardiomyocyte cross-sectional area, scale bar= 20μm (D). The error bars present ±SEM. *p* value was determined by two-tailed *t* test. WT, SMA (n=4).

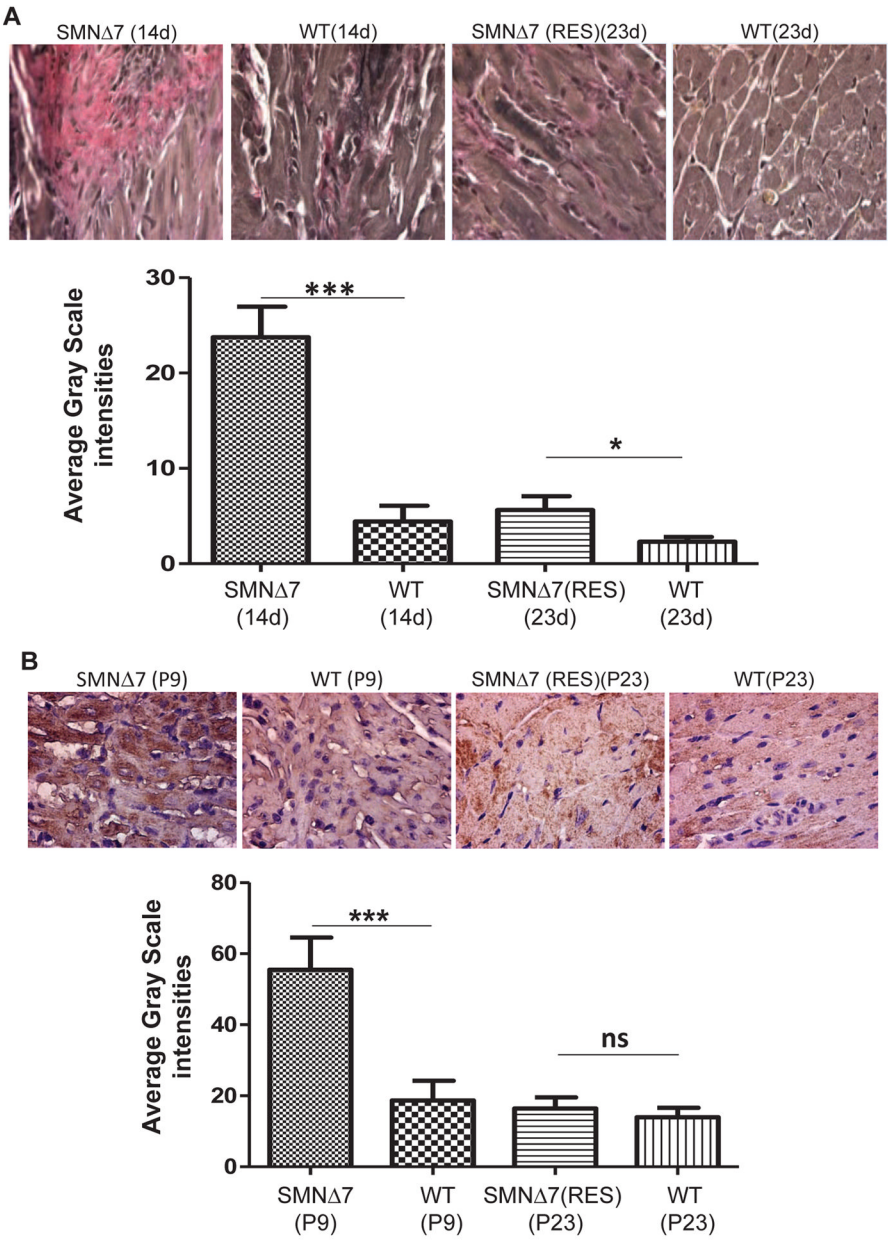

Figure 2.

Gene replacement therapy reduces interstitial fibrosis and 3-NT content. Representative images of VVG-stained cross-sections of heart in untreated SMNΔ7 at P14, rescued SMNΔ7 at P23, and age-matched wildtype littermates (A). VVG stains collagen type III pink and intensity of the pink area, represented as percentage of total area, is indication of collagen type III deposition. Representative images showing 3-nitrotyrosine (3-NT) immunostaining in the myocardium of untreated, treated SMNΔ7, and age matched wildtype mice (B). 3-NT content was quantified by measuring the average grayscale intensity in total area. The error bars present ±SEM and *P* value was determined by two-tailed *t* test. WT, SMA (n=4).

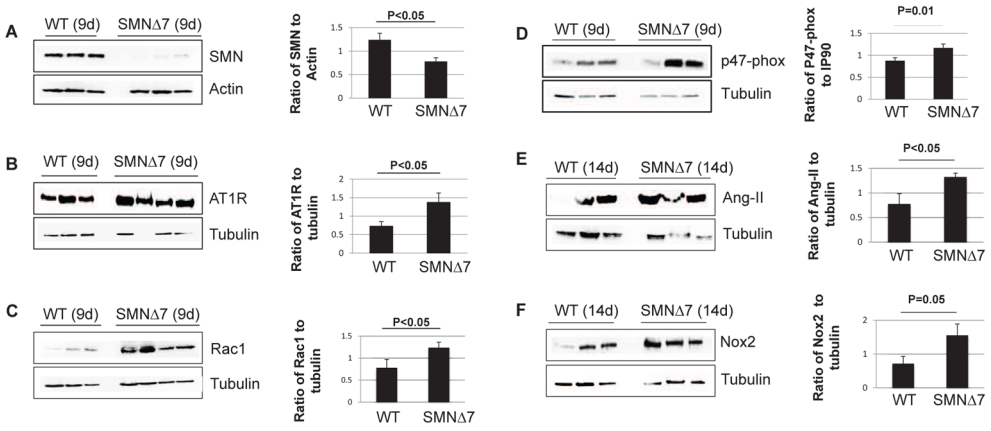

Figure 3.

Loss of SMN in the heart leads to activation of NADPH-oxidase. Western blot analysis of the heart extracts in SMNΔ7 mice indicate that very low levels of SMN (A) results in a significant increase in the levels of AT1R (B), Rac1 (C), P47-phox (D), Ang-II (E), and Nox2 (F) compared to wild type littermates at P9 or 14. The error bars present ±SE and *P* value was determined by two-tailed *t* test.

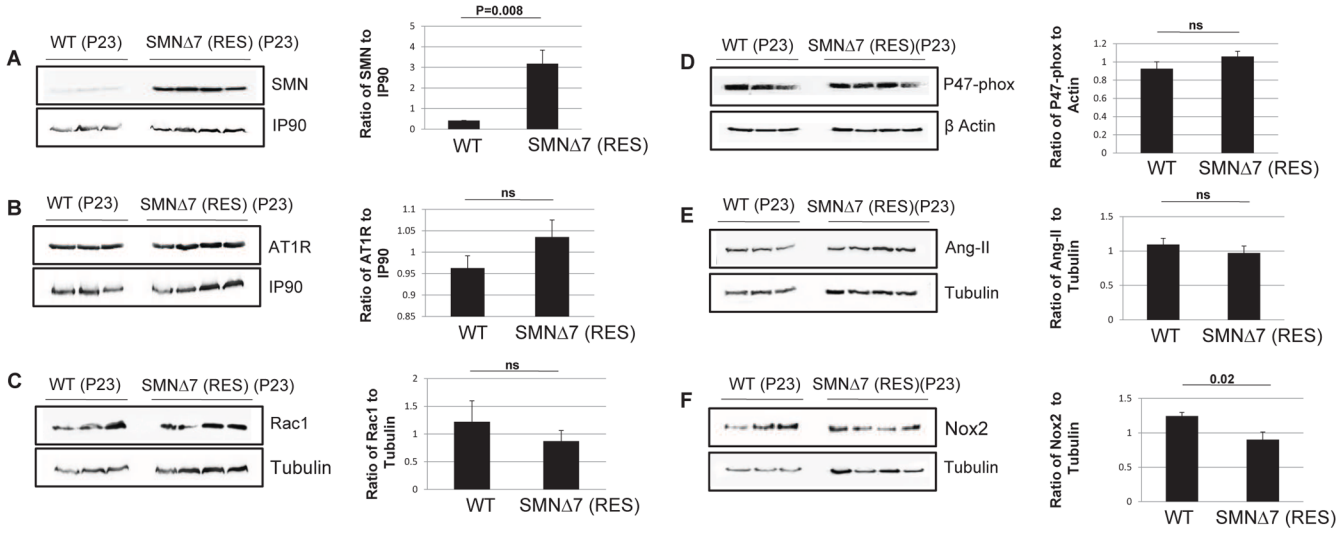

Figure 4.

Restoration of SMN in the heart returns the NADPH-oxidase biomarkers to normal levels. Western blot analysis of the heart extracts in rescued SMNΔ7 mice at P23 indicate high levels of SMN (A), and comparable levels of AT1R (B), Rac1 (C), P47-phox (D), Ang-II (E), and Nox2 (F) compared to age-matched wildtype littermates. The error bars present ±SE and *P* value was determined by two-tailed *t* test.

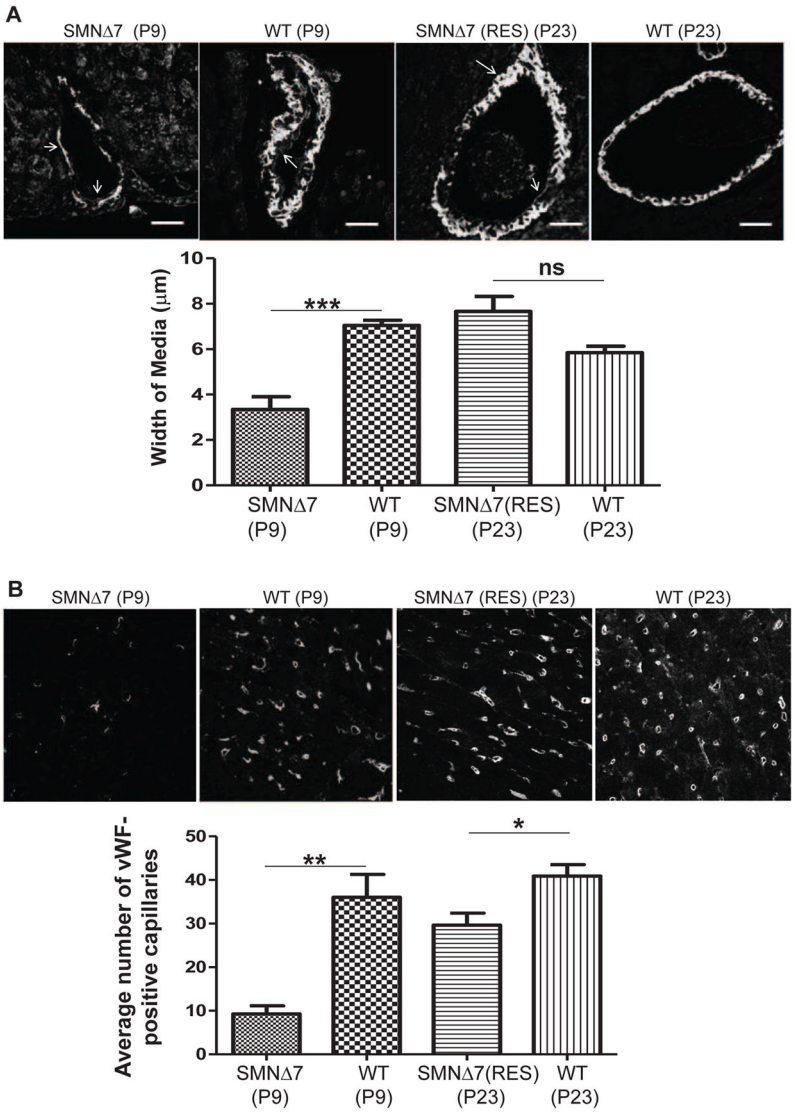

Figure 5.

Gene replacement therapy improves vascular impairments. Representative confocal images indicating arterioles (A) and capillaries (B) in the heart of untreated SMNΔ7 at P9, rescued SMNΔ7 at P23, and age matched wildtypes. Arterioles were double stained with eNOS (arrows pointing inward) to distinguish intima and α-smooth muscle actin (arrows pointing outward) to specify media; medial thickness was quantified by metamorphic analysis. Scale bar=20μm (A). Following vWF immuno-staining, average Number of vWF-positive capillaries was quantified in total area (B). The error bars present ±SEM and *P* value was determined by two-tailed *t* test. WT, SMA (n=4).

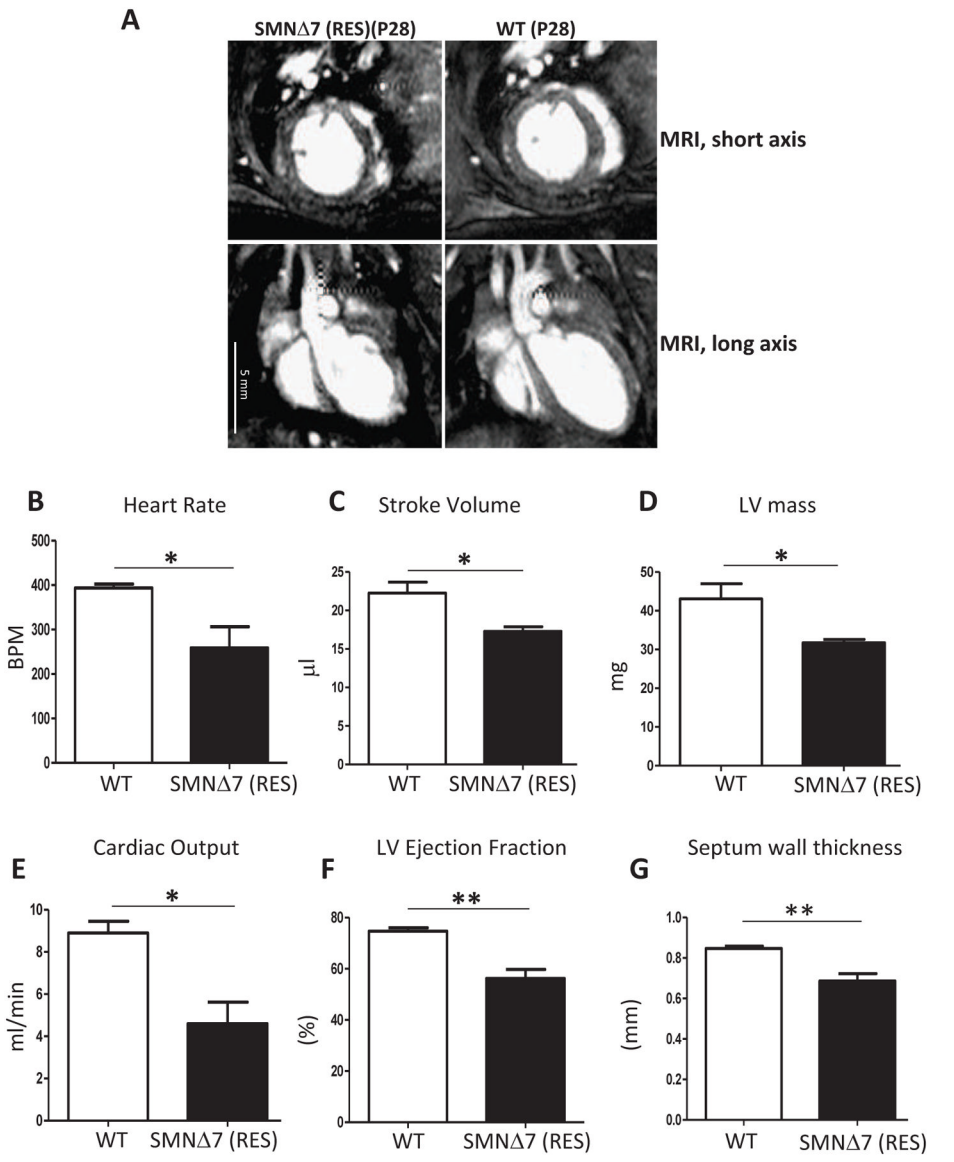

Figure 6.

Cardiac function of rescued SMA mice is significantly weaker than wildtype littermates. Long and short axis images of cardiac MRI of rescued SMNΔ7 mice and age-matched wildtypes at P28 (A). The heart rate was assessed through ECG monitoring during cardiac MRI (B). Left ventricle volumes (ml) at end diastole (*EDV*) and end systole (*ESV*) were quantified by Segment and stroke volume (C), cardiac Output (E), and LV ejection fraction (F) were determined. The stroke volume was calculated by subtracting the end-systolic volume from the end-diastolic volume (*SV = EDV – ESV)*. LV ejection fraction was calculated by the formula (*SV/EDV×100*). Cardiac output was determined by multiplying the heart rate to stroke volume. To calculate LV mass (D), the epicardial volumes were subtracted from endocardial volumes for all the slices from base to apex and myocardial specific gravity of 1.05 g/ml was multiplied to convert the volumes to masses. Septal wall thickness (G) was determined using a short axis midventricular slice at the end diastolic phase and averaging 5 measurements per heart. The error bars present ±SEM and *P* value was determined by two-tailed *t* test. WT, SMA (n=4).